Supporting Information for

Surface urban heat island across 419 global big cities

Shushi Peng[1], Shilong Piao[1*], Philippe Ciais[2], Pierre Friedlingstein[3], Catherine Ottle[2], François-Marie Bréon[2], Ranga B. Myneni[4]

[1] Department of Ecology, College of Urban and Environmental Sciences, Peking University, Beijing 100871, China

[2] Laboratoire des Sciences du Climat et de l'Environnement, CEA CNRS UVSQ, 91191 Gif-sur-Yvette, France

[3] School of Engineering, Computing and Mathematics, University of Exeter, Exeter EX4 4QF, UK

[4] Department of Geography and Environment, Boston University, Boston, MA 02215 USA

[*] To whom correspondence should be addressed. Email: slpiao@pku.edu.cn

This file includes

SI Text

References

Figure S1-S6

14 pages

Detailed methods

Determinate urban and suburban area

We used the MODIS land surface temperature (LST) Version 5 products MYD11A2 (http://modis-land.gsfc.nasa.gov/temp.htm), which is retrieved from clear sky observations using a generalized split-window algorithm.[1] Recently, these MODIS LST products are widely used in urban heat island and other earth science studies.[2-5] There are more details about MODIS LST products in the MODIS PI maintained products website (http://www.icess.ucsb.edu/modis/modis-lst.html). The MODIS Global Land Cover Map[6] defined the land cover type based on the IGBP land cover classifications. The "urban" pixels are defined as land covered by buildings and other man-made structures.

We first used City Clustering Algorithm[7] to determine the urban area for each big city. We defined the suburban area as the buffer zone that is a percentage (50%, 100% and 150%) of the urban area around the urban area. The detailed algorithm for the urban and suburban area determination is as follows:

Step 1. Enqueue the pixel of the location for each big city, which was determined from a geographical database [8] as the root node into the search queue.

Step 2. Dequeue a node and examine the eight neighbours around it. If the land cover type of the neighbouring pixel is urban land cover, add the neighbouring pixel into the queue, and assign attribute of the neighbouring pixel as an urban pixel, otherwise assign attribute of the neighbouring pixel as a non-urban pixel.

Step 3. If the queue is empty, every pixel in the queue has been examined – quit the search and return the urban map, otherwise repeat from Step 2.

Step 4. After the urban map is returned, suburban area are defined as the buffer zone, which is a percentage (50%, 100% and 150%) of the urban area around the urban centre based on the distances of the non-urban pixels to the urban map edge.

Taking Beijing as an example, Figure 1 shows the Beijing land cover map and the urban area map with three different suburban regions for areas are 50%, 100% and 150% of Beijing urban area around Beijing urban area. To test the impact of different suburban area on SUHII, we also calculated SUHII from a smaller suburban area (as 50% of urban area) and a larger suburban area (as 150% of urban area) and found that the SUHII are similar as SUHII derived from the suburban area equal to urban area (as 100% of urban area) (Figure S1). We test all the analysis with the smaller suburban area (as 50% of urban area) and larger suburban area (as 150% of urban area), and our conclusions are the same if the smaller suburban area (as 50% of urban area) or the larger suburban area (as 150% of urban area) are used.

Different drivers for daytime and nighttime SUHII and their seasonality

Figure S2-S5 shows the different divers for daytime and nighttime SUHII. Figure S2 shows that the vegetation fraction and EVI are the most important drivers for daytime SUHII.[9-12] Nighttime SUHII is more related to albedo and nighttime light (Figure S3).[13,14] The seasonal amplitude of daytime SUHII (summer daytime SUHII minus winter daytime SUHII) is driven by vegetation activity seasonality (EVI seasonality) (Figure S4), while the seasonal amplitude of nighttime SUHII is more negatively correlated with MT0 which is latitudinal pattern (higher in tropic and lower in high latitude regions). The results of Figure S2-S5 are summarized in Figure 4.

Figure S6 shows the spatial patterns of summer and winter daytime and nighttime SUHII. In temperate regions in North Hemisphere, the summer daytime SUHII is larger than winter daytime SUHII, summer daytime SUHII is similar with winter daytime SUHII in tropical regions (Figure S6). Figure S6 is the source of the seasonal amplitude of daytime and nighttime SUHII shown in Figure 5.

References

(1) Wan, Z.; Zhang, Y.; Zhang, Q.; Li, Z. L., Quality assessment and validation of the MODIS global land surface temperature. *Int. J. Remote Sens.* **2004**, *25* (1), 261-274.

(2) Imhoff, M. L.; Zhang, P.; Wolfe, R. E.; Bounoua, L., Remote sensing of the urban heat island effect across biomes in the continental USA. *Remote Sens. Environ.* **2010,** *114* (3), 504-513.

(3) Jin, M.; Dickinson, R. E., Land surface skin temperature climatology: benefitting from the strengths of satellite observations. *Environ. Res. Lett.* **2010,** *5* (4), 044004.

(4) Sims, D. A.; Rahman, A. F.; Cordova, V. D.; El-Masri, B. Z.; Baldocchi, D. D.; Bolstad, P. V.; Flanagan, L. B.; Goldstein, A. H.; Hollinger, D. Y.; Misson, L.; Monson, R. K.; Oechel, W. C.; Schmid, H. P.; Wofsy, S. C.; Xu, L., A new model of gross primary productivity for North American ecosystems based solely on the enhanced vegetation index and land surface temperature from MODIS. *Remote Sens. Environ.* **2008**, *112* (4), 1633-1646.

(5) Zhang, P.; Imhoff, M. L.; Wolfe, R. E.; Bounoua, L., Characterizing urban heat islands of global settlements using MODIS and nighttime lights products. *Can. J. Remote Sens.* **2010,** *36* (3), 185-196.

(6) Friedl, M. A.; McIver, D. K.; Hodges, J. C. F.; Zhang, X. Y.; Muchoney, D.; Strahler, A. H.; Woodcock, C. E.; Gopal, S.; Schneider, A.; Cooper, A.; Baccini, A.; Gao, F.; Schaaf, C., Global land cover mapping from MODIS: algorithms and early results. *Remote Sens. Environ.* **2002,** *83* (1-2), 287-302.

(7) Rozenfeld, H. D.; Rybski, D.; Andrade, J. S.; Batty, M.; Stanley, H. E.; Makse, H. A., Laws of population growth. *Proc. Natl. Acad. Sci.* **2008,** *105* (48), 18702-18707.

(8) http://www.geonames.org.

(9) Roth, M.; Oke, T. R.; Emery, W. J., Satellite-derived urban heat islands from three coastal cities and utilization of such data in urban climatology. *Int. J. Remote Sens.*, **1989**, *10*, 1699–1720.

(10) Hung, T.; Uchihama, D.; Ochi, S.; Yasuoka, Y., Assessment with satellite data of the urban heat island effects in Asian mega cities. *Int. J. Appl. Earth Obs. Geoinf.* **2006,** *8*, 34-48.

(11) Weng, Q. H.; Lu, D. S.; Schubring, J., Estimation of land surface temperature-vegetation abundance relationship for urban heat island studies. *Remote Sens. Environ.* **2004,** *89* (4), 467-483.

(12) Hu, Y.; Jia, G., Influence of land use change on urban heat island derived from multi-sensor data. *Int. J. Climatol.* **2010,** *30* (9), 1382-1395.

(13) Oke, T. R., The urban energy balance. *Prog. Phys. Geog.* **1988,** *12* (4), 471-508.

(14) Arnfield, A. J., Two decades of urban climate research: A review of turbulence, exchanges of energy and water, and the urban heat island. *Int. J. Climatol.* **2003**, *23* (1), 1-26.

Supporting Information Figure Legends

Figure S1. Comparisons of daytime (nighttime) SUHII derived from urban LST minus different suburban areas' LST. Comparison between daytime SUHII derived when suburban area equal to the urban area (Daytime $SUHII_{100\%}$) and (A) daytime SUHII derived when suburban area is 50% of urban area (Daytime $SUHII_{50\%}$) and (B) daytime SUHII derived when suburban area is 150% of urban area (Daytime $SUHII_{150\%}$); comparison between nighttime SUHII derived when suburban area is equal to urban area (Nighttime $SUHII_{100\%}$) and (C) nighttime SUHII derived when suburban area is 50% of urban area (Nighttime $SUHII_{50\%}$) and (D) nighttime SUHII derived when suburban area is 150% of urban area (Nighttime $SUHII_{150\%}$).

Figure S2. Spatial relationships of annual daytime SUHII with independent variables in Figure 4. Relationships between annual daytime SUHII and (A) the difference in VCF between urban and suburban (δVCF), (B) the difference in EVI between urban and suburban (δEVI), (C) the difference in white sky albedo (WSA) between urban and suburban (δWSA), (D) the difference in nighttime light (NL) between urban and suburban (δNL), (E) the difference in population density (PD) between urban and suburban (δPD), (F) mean annual temperature (MAT), (G) mean annual precipitation (MAP), (H) mean temperature for the months which air temperature exceed 0°C (MT0), (I) the sum of pixels of the urban area (P_{city}), (J) seasonal amplitude of δEVI ($A_{\delta EVI}$), (K) seasonal amplitude of δWSA ($A_{\delta WSA}$) and (L) seasonal amplitude of temperature (A_T).

Figure S3. Spatial relationships of annual nighttime SUHII with independent variables in Figure 4. Relationships between annual daytime SUHII and (A) the difference in VCF between urban and suburban (δVCF), (B) the difference in EVI between urban and suburban (δEVI), (C) the difference in white sky albedo (WSA) between urban and suburban (δWSA), (D) the difference in nighttime light (NL) between urban and suburban (δNL), (E) the difference in population density (PD) between urban and suburban (δPD), (F) mean annual temperature (MAT), (G) mean annual precipitation (MAP), (H) mean temperature for the months which air temperature exceed 0°C (MT0), (I) the sum of pixels of the urban area (P_{city}), (J) seasonal amplitude of δEVI ($A_{\delta EVI}$), (K) seasonal amplitude of δWSA ($A_{\delta WSA}$) and (L) seasonal amplitude of temperature (A_T).

Figure S4. Spatial relationships of daytime SUHII seasonal amplitude ($A_{Daytime\ SUHII}$) with independent variables in Figure 4. Relationships between annual daytime SUHII and (A) the difference in VCF between urban and suburban (δVCF), (B) the difference in EVI between urban and suburban (δEVI), (C) the difference in white sky albedo (WSA) between urban and suburban (δWSA), (D) the difference in nighttime light (NL) between urban and suburban (δNL), (E) the difference in population density (PD) between urban and suburban (δPD), (F) mean annual temperature (MAT), (G) mean annual precipitation (MAP), (H) mean temperature for the months which air temperature exceed 0°C (MT0), (I) the sum of pixels of the urban area (P_{city}), (J) seasonal amplitude of δEVI ($A_{\delta EVI}$), (K) seasonal amplitude of δWSA ($A_{\delta WSA}$) and (L) seasonal amplitude of temperature (A_T).

Figure S5. Spatial relationships of nighttime SUHII seasonal amplitude ($A_{Nighttime\ SUHII}$) with independent variables in Figure 4. Relationships between annual daytime SUHII and (A) the difference in VCF between urban and suburban (δVCF), (B) the difference in EVI between urban and suburban (δEVI), (C) the difference in white sky albedo (WSA) between urban and suburban (δWSA), (D) the difference in nighttime light (NL) between urban and suburban (δNL), (E) the difference in population density (PD) between urban and suburban (δPD), (F) mean annual temperature (MAT), (G) mean annual precipitation (MAP), (H) mean temperature for the months which air temperature exceed 0°C (MT0), (I) the sum of pixels of the urban area (P_{city}), (J) seasonal amplitude of δEVI ($A_{\delta EVI}$), (K) seasonal amplitude of δWSA ($A_{\delta WSA}$) and (L) seasonal amplitude of temperature (A_T).

Figure S6. Spatial patterns of (A) summer daytime SUHII, (B) summer nighttime SUHII, (C) winter daytime SUHII and (D) winter nighttime SUHII averaged over the period 2003-2008 across 419 global big cities.

Figure S1. Comparisons of daytime (nighttime) SUHII derived from urban LST minus different suburban areas' LST. Comparison between daytime SUHII derived when suburban area equal to the urban area (Daytime $SUHII_{100\%}$) and (A) daytime SUHII derived when suburban area is 50% of urban area (Daytime $SUHII_{50\%}$) and (B) daytime SUHII derived when suburban area is 150% of urban area (Daytime $SUHII_{150\%}$); comparison between nighttime SUHII derived when suburban area is equal to urban area (Nighttime $SUHII_{100\%}$) and (C) nighttime SUHII derived when suburban area is 50% of urban area (Nighttime $SUHII_{50\%}$) and (D) nighttime SUHII derived when suburban area is 150% of urban area (Nighttime $SUHII_{150\%}$).

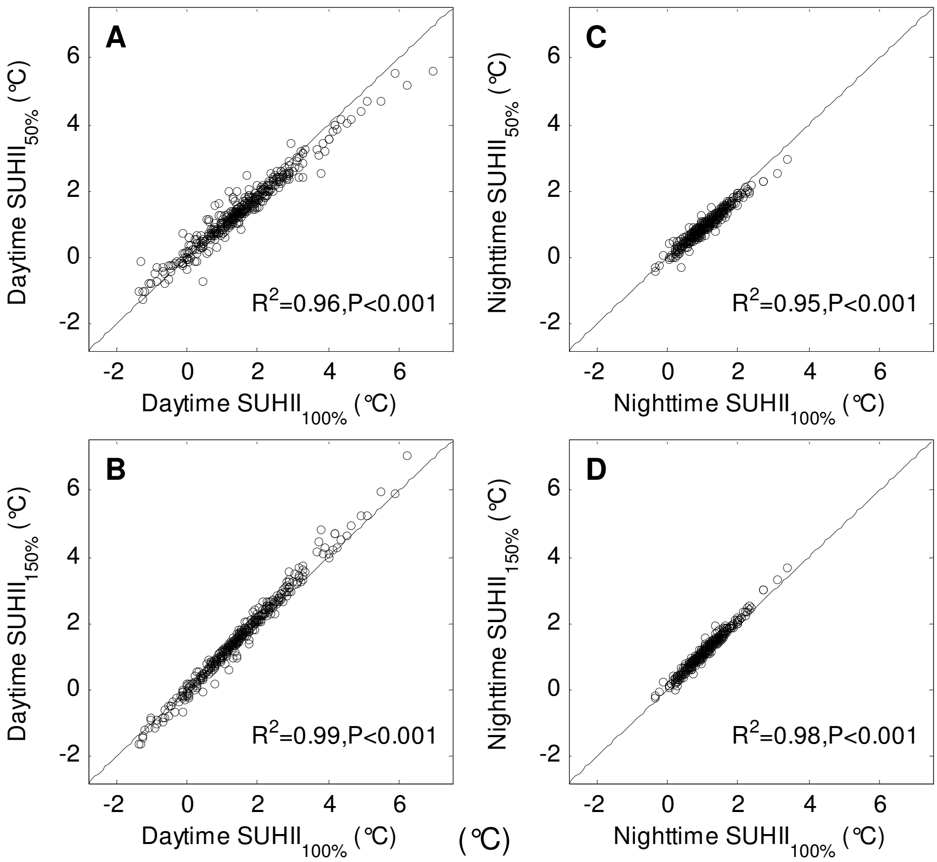

Figure S2. Spatial relationships of annual daytime SUHII with independent variables in Figure 4. Relationships between annual daytime SUHII and (A) the difference in VCF between urban and suburban (δVCF), (B) the difference in EVI between urban and suburban (δEVI), (C) the difference in white sky albedo (WSA) between urban and suburban (δWSA), (D) the difference in nighttime light (NL) between urban and suburban (δNL), (E) the difference in population density (PD) between urban and suburban (δPD), (F) mean annual temperature (MAT), (G) mean annual precipitation (MAP), (H) mean temperature for the months which air temperature exceed 0°C (MT0), (I) the sum of pixels of the urban area (P_{city}), (J) seasonal amplitude of δEVI ($A_{\delta EVI}$), (K) seasonal amplitude of δWSA ($A_{\delta WSA}$) and (L) seasonal amplitude of temperature (A_T).

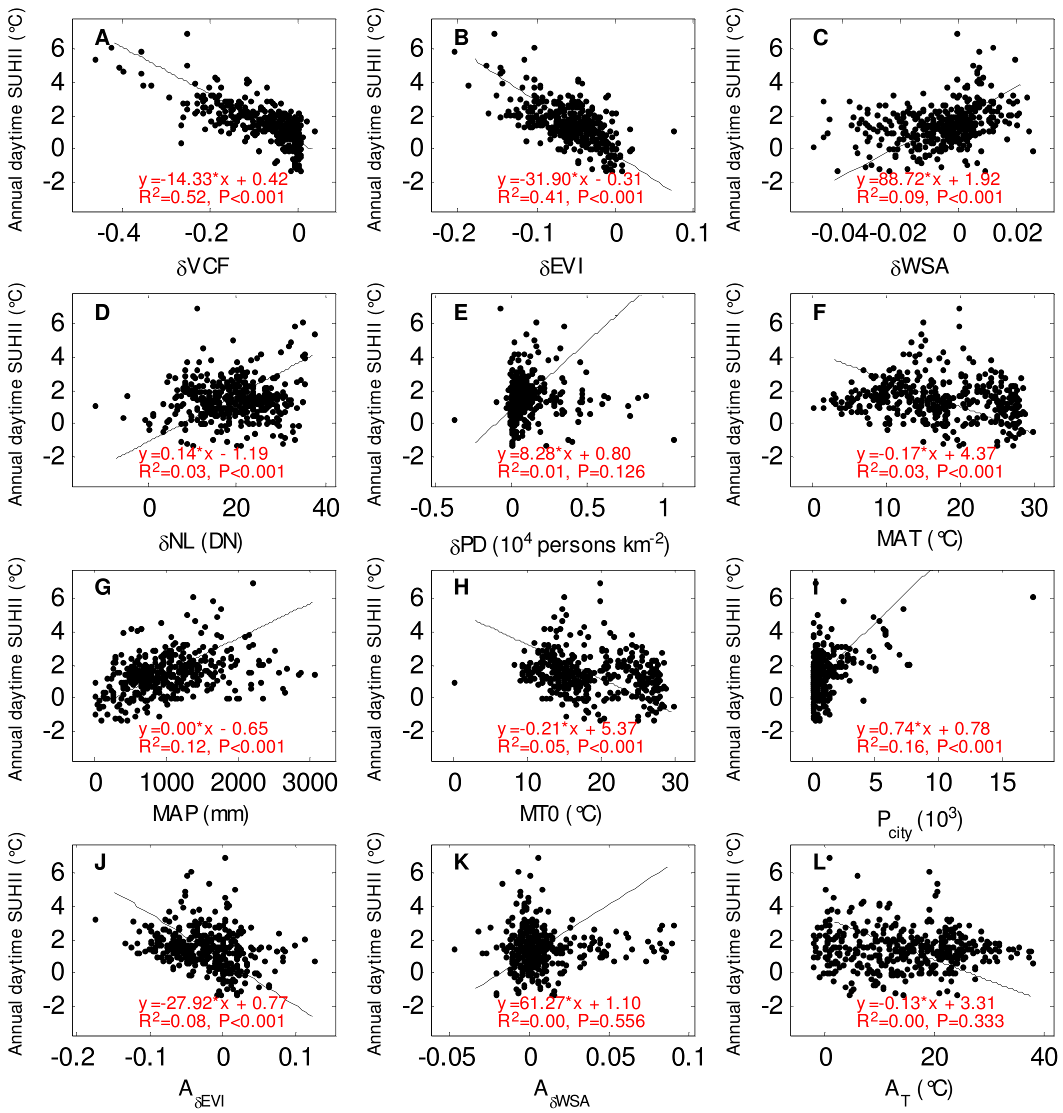

Figure S3. Spatial relationships of annual nighttime SUHII with independent variables in Figure 4. Relationships between annual daytime SUHII and (A) the difference in VCF between urban and suburban (δVCF), (B) the difference in EVI between urban and suburban (δEVI), (C) the difference in white sky albedo (WSA) between urban and suburban (δWSA), (D) the difference in nighttime light (NL) between urban and suburban (δNL), (E) the difference in population density (PD) between urban and suburban (δPD), (F) mean annual temperature (MAT), (G) mean annual precipitation (MAP), (H) mean temperature for the months which air temperature exceed 0°C (MT0), (I) the sum of pixels of the urban area (P_{city}), (J) seasonal amplitude of δEVI ($A_{\delta EVI}$), (K) seasonal amplitude of δWSA ($A_{\delta WSA}$) and (L) seasonal amplitude of temperature (A_T).

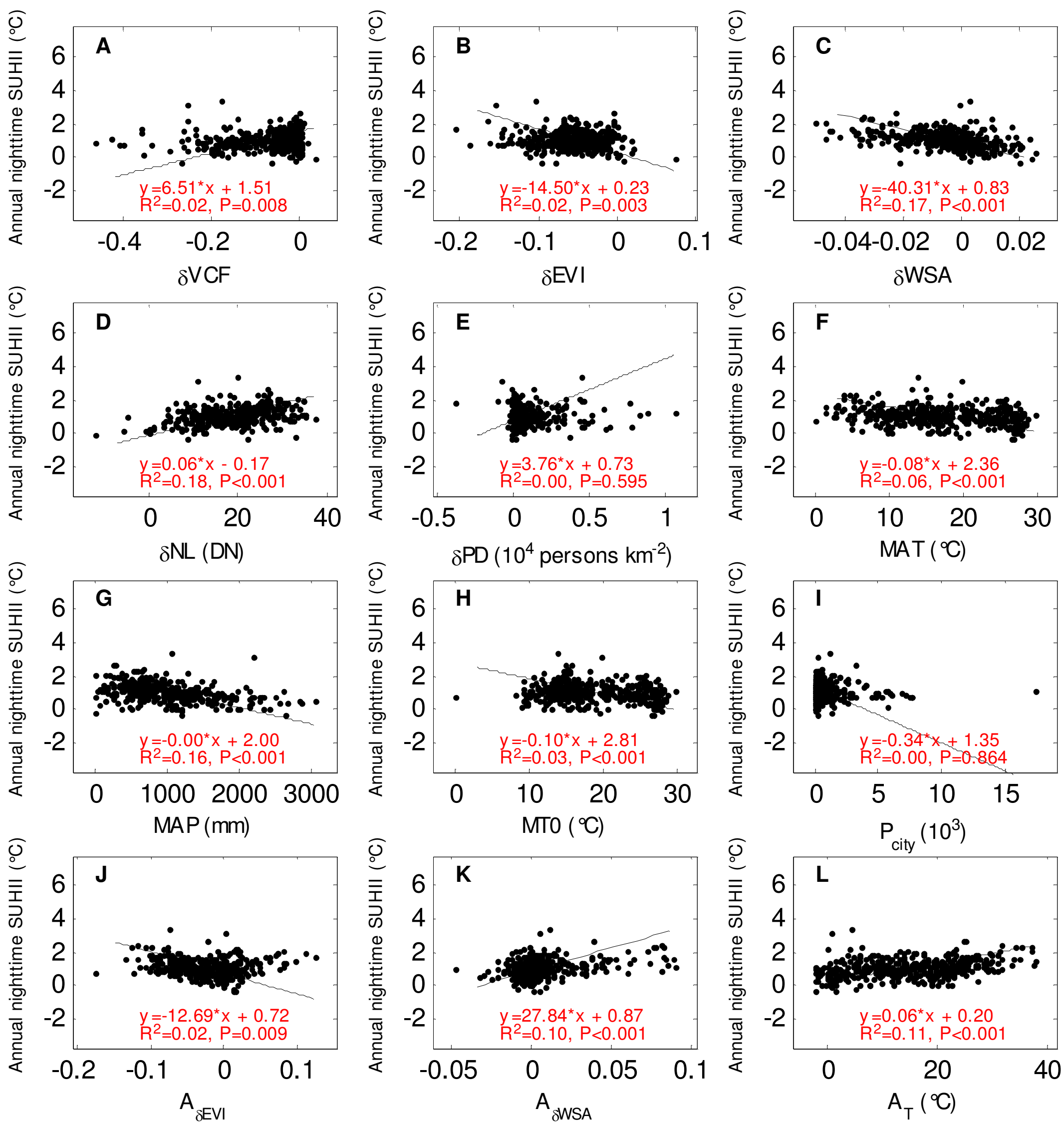

Figure S4. Spatial relationships of daytime SUHII seasonal amplitude ($A_{Daytime\ SUHII}$) with independent variables in Figure 4. Relationships between annual daytime SUHII and (A) the difference in VCF between urban and suburban (δVCF), (B) the difference in EVI between urban and suburban (δEVI), (C) the difference in white sky albedo (WSA) between urban and suburban (δWSA), (D) the difference in nighttime light (NL) between urban and suburban (δNL), (E) the difference in population density (PD) between urban and suburban (δPD), (F) mean annual temperature (MAT), (G) mean annual precipitation (MAP), (H) mean temperature for the months which air temperature exceed 0°C (MT0), (I) the sum of pixels of the urban area (P_{city}), (J) seasonal amplitude of δEVI ($A_{\delta EVI}$), (K) seasonal amplitude of δWSA ($A_{\delta WSA}$) and (L) seasonal amplitude of temperature (A_T).

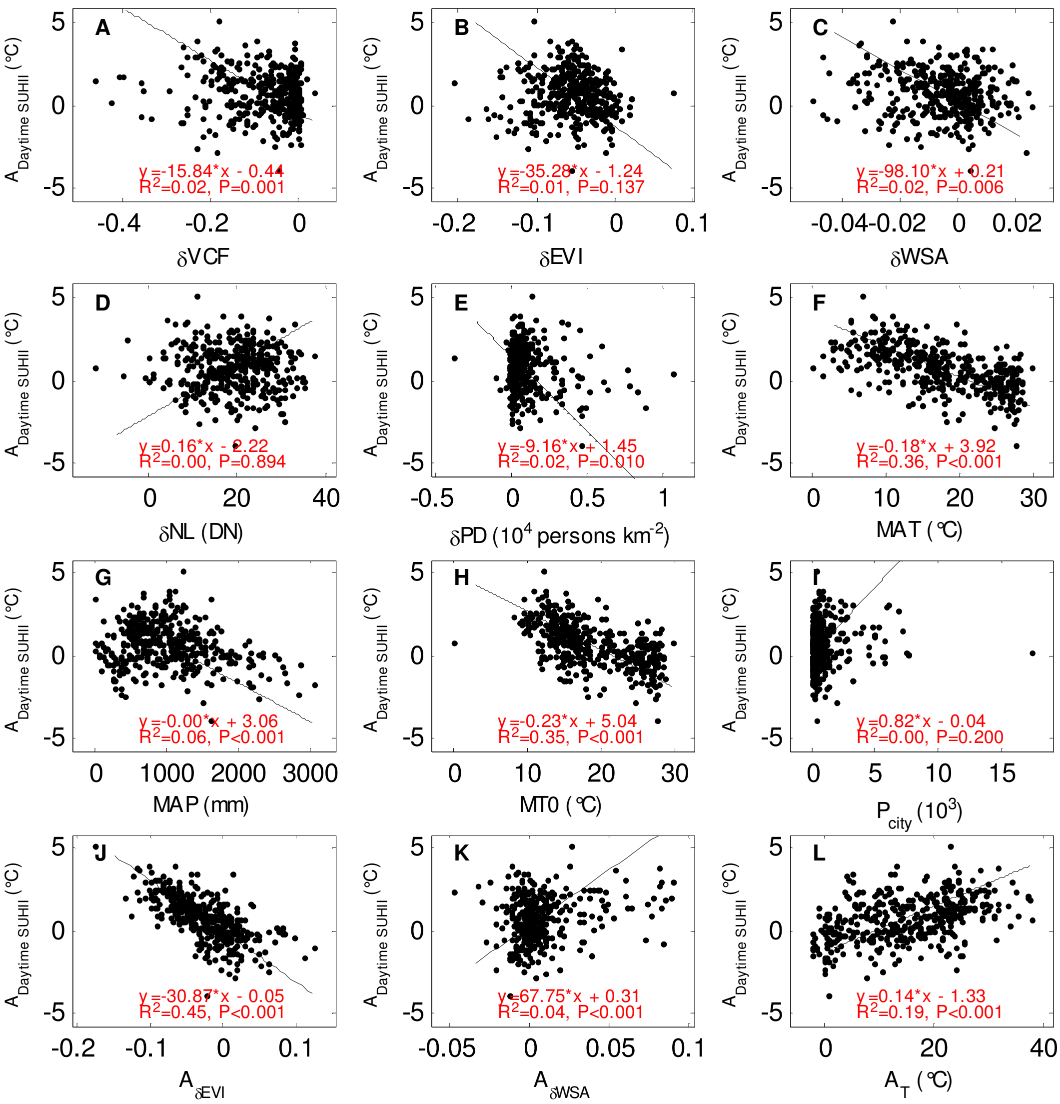

Figure S5. Spatial relationships of nighttime SUHII seasonal amplitude ($A_{Nighttime\ SUHII}$) with independent variables in Figure 4. Relationships between annual daytime SUHII and (A) the difference in VCF between urban and suburban (δVCF), (B) the difference in EVI between urban and suburban (δEVI), (C) the difference in white sky albedo (WSA) between urban and suburban (δWSA), (D) the difference in nighttime light (NL) between urban and suburban (δNL), (E) the difference in population density (PD) between urban and suburban (δPD), (F) mean annual temperature (MAT), (G) mean annual precipitation (MAP), (H) mean temperature for the months which air temperature exceed 0°C (MT0), (I) the sum of pixels of the urban area (P_{city}), (J) seasonal amplitude of δEVI ($A_{\delta EVI}$), (K) seasonal amplitude of δWSA ($A_{\delta WSA}$) and (L) seasonal amplitude of temperature (A_T).

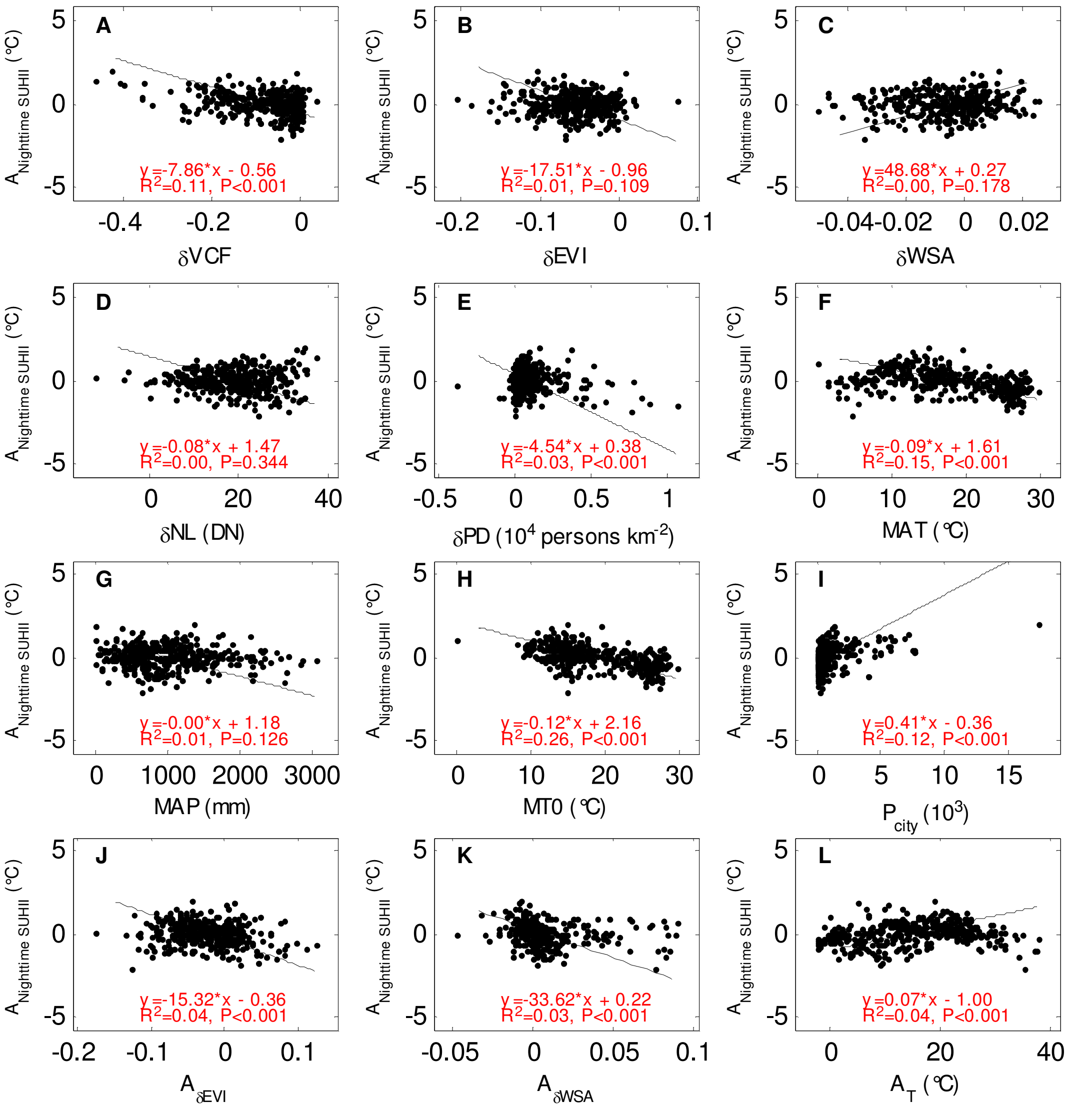

Figure S6. Spatial patterns of (A) summer daytime SUHII, (B) summer nighttime SUHII, (C) winter daytime SUHII and (D) winter nighttime SUHII averaged over the period 2003-2008 across 419 global big cities.